Japanese Journal of Applied Physics
Vol. 43, No. 8A, 2004, pp. 5469–5476
©2004 The Japan Society of Applied Physics

Modeling of Strain Induced by Compositional Variation in Wafer-Shaped Bulk Mixed Crystals

Md. Rafiqul ISLAM[1], Prabhat VERMA[2], Akira HIROKI[1,3] and Masayoshi YAMADA[1,3]*

[1]*Division of Information and Production Science, Graduate School of Engineering and Science, Kyoto Institute of Technology, Matsugasaki, Sakyo-ku, Kyoto 606-8585, Japan*
[2]*Department of Applied Physics, Osaka University, Osaka 565-0871, Japan*
[3]*Department of Electronics and Information Science, Kyoto Institute of Technology, Matsugasaki, Sakyo-ku, Kyoto 606-8585, Japan*

(Received January 7, 2004; accepted April 13, 2004; published August 10, 2004)

A radially symmetrical strain model has been proposed to determine the residual strain distribution induced by compositional variation in wafer-shaped bulk mixed crystals. The strain components in cylindrical coordinates are analytically derived by assuming a symmetrical variation of composition along the radial direction and uniform composition along the growth direction. The results obtained from the model demonstrated that the quantitative amount of strain and its distribution are highly dependent on the radial compositional profile and its range. The strain model is confirmed with the combination of micro-Raman scattering and optical transmission experiments, which were performed in single-crystalline $Si_{1-x}Ge_x$ mixed material grown by the floating zone method. The experimental results indicated that there exists residual strain due to the compositional variation along the radial direction in $Si_{1-x}Ge_x$ wafers, which is well explained by the strain model proposed here. [DOI: 10.1143/JJAP.43.5469]

KEYWORDS: stress–strain analysis, radial compositional variation, wafer-shaped bulk mixed crystal

1. Introduction

Bulk mixed crystals such as $Si_{1-x}Ge_x$ are attractive materials for advanced electronic and optoelectronic device applications. Many applications of $Si_{1-x}Ge_x$ mixed crystals are critically dependent on compositional variation. For instance, compositionally gradient $Si_{1-x}Ge_x$ can be used as focusing and diffracting monochromator crystals for X-ray and synchrotron radiation[1–3] as well as it can be used as buffer layers in high-performance CMOS transistors.[4] In these applications, lattice spacing is a vital factor, which can be modified due to strain induced by compositional variation in the bulk mixed crystal system.[5,6] It is therefore important to determine the quantitative amount of strain for understanding lattice spacing under compositional variation in bulk mixed crystals. To our knowledge, no research work has been carried out on residual strain induced by compositional variation in the bulk mixed crystal system. Recently, we have developed an axially symmetrical strain model,[6] which can be applied to determine the quantitative amount of strain and its distribution in bulk mixed crystals for a simultaneous variation of composition along the growth and radial directions. In order to determine the quantitative amount of strain and its distribution for a symmetrical variation of composition along the radial direction and uniform composition along the growth direction in wafer-shaped bulk mixed crystals, a radially symmetrical strain model has been proposed in the present study. The results obtained from the model for various compositional profiles in bulk $Si_{1-x}Ge_x$ mixed crystal have been presented as an example. Furthermore, micro-Raman scattering (MRS) and optical transmission (OT) measurements have been carried out in various wafer-shaped samples, which were prepared from a bulk $Si_{1-x}Ge_x$ crystal grown by the floating zone method. The results obtained from the MRS and OT experiments have been compared to confirm the model proposed here.

*E-mail address: yamada@dj.kit.ac.jp

2. Modeling, Analytical Solution, and Numerical Calculation of Strain in Wafer-Shaped Bulk Mixed Crystals

2.1 Radially symmetrical strain model

The lattice spacing in bulk mixed crystals depends on the compositional fraction and should be uniform under homogeneous composition. On the other hand, if composition varies, the lattice spacing would be changed depending on the compositional profile. For a symmetrical variation of composition along the r axis while a uniform composition along the z axis of a wafer-shaped crystal, the deformation of lattice spacing can be realized from Fig. 1. The composition-dependent continuous change in lattice spacing causes residual strain in bulk mixed crystals, which can be expressed[6] by

$$\varepsilon[x(r) - x_c] = \alpha_l[x(r)]x(r) - \alpha_{lc}x_c, \quad (1)$$

where $x(r)$ is the compositional variation along the radial direction. x_c is the composition and α_{lc} is the rate of change in lattice spacing at the center of the wafer, respectively. The rate of change in lattice spacing, α_l, can be expressed[6] by

$$\alpha_l[x(r)] = \frac{1}{a[x(r)]}\frac{da[x(r)]}{dx(r)}, \quad (2)$$

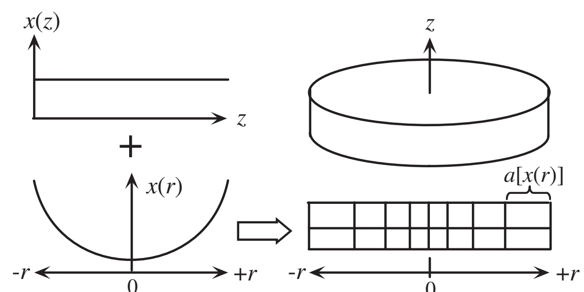

Fig. 1. Lattice spacing change by the parabolic-like compositional variation along the r axis and uniform composition along the z axis.

where $a[x(r)]$ is the compositional dependence of lattice spacing. The state of strain in bulk mixed crystals entirely depends on the compositional profile. Under a symmetrical compositional variation along the r axis and a uniform composition along the z axis of a wafer-shaped crystal, radial and tangential strains may remain. Consequently, in-plane strain can be assumed in the crystal. Although well known epilayer strain models[7–10] have been used to solve the in-plane strain issues in epilayers, they cannot be applied to evaluate the strain in bulk mixed crystals, because strain in epilayers is induced by the abrupt change in lattice constant, which is not the case in bulk mixed crystals. However, the proposed strain model can be applied to investigate the strain in epilayers as well as in bulk mixed crystals.

2.2 *Analytical solution in cylindrical coordinates*

By assuming a symmetrical variation of composition along the r axis and a uniform composition along the z axis in isotropic materials, the shear stress components and the stress along the z axis can be neglected. Thus, the stress equation in cylindrical coordinates[11] is reduced to

$$\frac{d\sigma_{rr}}{dr} + \frac{\sigma_{rr} - \sigma_{\theta\theta}}{r} = 0, \tag{3}$$

where σ_{rr} and $\sigma_{\theta\theta}$ are the stress components along the radial and the tangential directions, respectively. The variable r lies within the range of $0 \le |r| \le r_0$, where r_0 is the radius of the wafer. If ε_{rr} is the actual radial strain, $\varepsilon_{rr} - \varepsilon[x(r) - x_c]$ represents the part due to stress. The radial and tangential strains can be expressed by $\varepsilon_{rr} = du(r)/dr$ and $\varepsilon_{\theta\theta} = u(r)/r$, where $u(r)$ is the radial displacement. Therefore, an ordinary stress–strain relationship[11] including the strain induced by compositional variation can be expressed by

$$\frac{du(r)}{dr} - \varepsilon[x(r) - x_c] = \frac{1}{E}[\sigma_{rr} - P\sigma_{\theta\theta}], \tag{4}$$

$$\frac{u(r)}{r} - \varepsilon[x(r) - x_c] = \frac{1}{E}[\sigma_{\theta\theta} - P\sigma_{rr}], \tag{5}$$

where E and P are the Young's modulus and Poisson's ratio, respectively. By using eqs. (4) and (5) along with eq. (3), the radial displacement can be expressed by

$$u(r) = (1+P)\frac{1}{r}\int_0^r \big(\alpha_l[x(r)]x(r) - \alpha_{lc}x_c\big) r\,dr + C_1 r + \frac{C_2}{r}, \tag{6}$$

where C_1 and C_2 are the integration constants. By substituting eq. (6) into eqs. (4) and (5), the stress components can be determined, which help in determining the constants C_1 and C_2 from the boundary conditions. At the center $r \to 0$, C_2 must be made to vanish in order that $u(r)$ may not be infinite. At the edge $r = r_0$, we must have $\sigma_{rr} = 0$. Thus the final expression of radial and tangential strain components can be given by

$$\begin{aligned}\varepsilon_{rr}(r) = {} & (1-P)\frac{1}{r_0^2}\int_0^{r_0} \big\{\alpha_l[x(r)]x(r) - \alpha_{lc}x_c\big\} r\,dr \\ & - (1+P)\frac{1}{r^2}\int_0^{r} \big\{\alpha_l[x(r)]x(r) - \alpha_{lc}x_c\big\} r\,dr \\ & + (1+P)\big\{\alpha_l[x(r)]x(r) - \alpha_{lc}x_c\big\},\end{aligned} \tag{7}$$

$$\begin{aligned}\varepsilon_{\theta\theta}(r) = {} & (1-P)\frac{1}{r_0^2}\int_0^{r_0} \big\{\alpha_l[x(r)]x(r) - \alpha_{lc}x_c\big\} r\,dr \\ & + (1+P)\frac{1}{r^2}\int_0^{r} \big\{\alpha_l[x(r)]x(r) - \alpha_{lc}x_c\big\} r\,dr.\end{aligned} \tag{8}$$

By using eqs. (7) and (8), the radial and tangential strain components can be determined if the compositional profile of the crystal is known. In order to apply the model for various compositional profiles, the composition function may be generally given in polynomial form:

$$x(r') = \left(x_c \pm \sum_{n=1}^{N} A_{2n}^n r'^{2n}\right), \tag{9}$$

where A_{2n}^n is a constant, by which we can adjust the range of composition along the radial direction. The shape of compositional profile can also be adjusted by the constant A_{2n}^n. Here, the normalized variables: $r' = r/r_0$ is introduced. The maximum numbers of N may be limited to fit the compositional profile.

2.3 *Numerical calculation of strain in bulk $Si_{1-x}Ge_x$*

In this study, the strain distributions are investigated in bulk $Si_{1-x}Ge_x$ mixed crystal as an example. The parameters to be used for $Si_{1-x}Ge_x$ are determined by linear interpolation between the values listed for Si and Ge crystals in Table I. By using eqs. (7)–(9), the radial and tangential strain distributions are evaluated for various compositional profiles. Here, the strain distributions are presented for the parabolic compositional profile and for the compositional profile with flat near the center, hereafter referred to as flat-center parabolic profile. These compositional profiles and the strain distributions evaluated from these profiles are shown in Figs. 2(a) and 2(b), and in Figs. 2(c) and 2(d), respectively. It is found in Figs. 2(c) and 2(d) that both radial and tangential strains increase at the center as well as along the radial direction with increasing composition from the center to the edge of the wafer. However, their quantitative amount is found to be higher for the parabolic profile than that for the flat-center parabolic profile. Figure 2(c) shows that the amount of radial strain varies from 3.59×10^{-4} to 1.08×10^{-3}, and from 1.4×10^{-3} to 4.3×10^{-3} for the parabolic compositional variation from 0 to 0.05 and from 0 to 0.20, respectively. For the same compositional profile and ranges, the tangential strain varies from 3.59×10^{-4} to 6.3×10^{-4} and from 1.4×10^{-3} to 2.4×10^{-3}. On the other hand, for the flat-center parabolic profile, the similar results are varied from 1.84×10^{-4} to 9.94×10^{-4} and from 8.80×10^{-4} to 4.1×10^{-3}, and from 1.84×10^{-4} to 3.93×10^{-4} and from 8.80×10^{-4} to 1.6×10^{-3} in Fig. 2(d). Although the radial and tangential strains are almost the same at the wafer center for each of the compositional profiles and ranges, the radial strain becomes higher than the tangential strain with increasing composition along the radial direction. Furthermore, the strain value is found to be approximately twofold higher at the wafer center

Table I. Physical constants in Si and Ge crystals.[12]

	Si	Ge
Lattice constant a (A°)	5.4311	5.6579
Poisson's ratio P	0.33	0.30

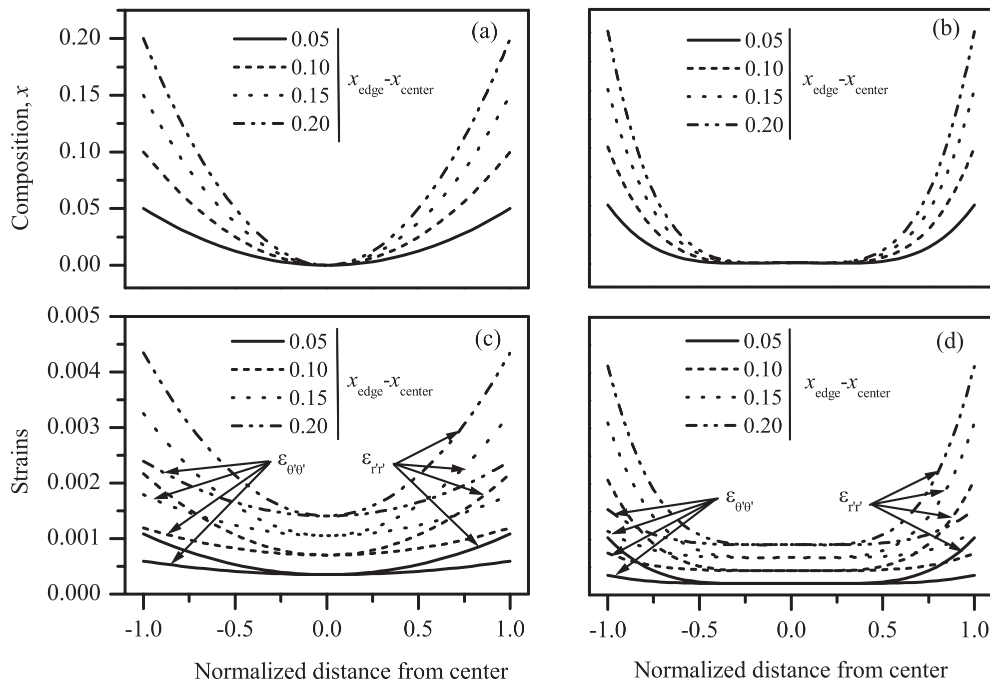

Fig. 2. Typical compositional profiles: (a) parabolic and (b) flat-center parabolic. Strain distributions induced in bulk $Si_{1-x}Ge_x$ mixed crystal for the (c) parabolic and (d) flat-center parabolic compositional profiles.

for the parabolic profile than that for the flat-center parabolic profile. However, its value is less than twofold higher at the wafer edge for both of the profiles. Therefore, the quantitative amount of strain and its distribution in bulk mixed crystals are strongly sensitive to the compositional profile and its range.

3. Experimental Confirmation of Strain Model

In order to confirm the present strain model, both MRS and OT experiments were carried out. Since a shift in optical phonons in MRS is induced by both strain and composition under compositional variation in bulk mixed crystals,[13–15] MRS is a good technique for investigating strain and composition. Furthermore, OT measurements should have the influence of strain because the electronic energy bands are modified by the strain.[16,17] Therefore, MRS and OT could be a good combination to confirm the model proposed here.

3.1 Experimental procedure

The $Si_{1-x}Ge_x$ single crystal investigated here was grown by a modified floating-zone technique.[18] The length of the crystal was approximately 20 cm and the diameter varied from 11 to 18 mm. The composition of Ge was gradually increased from zero at the ⟨111⟩ Si seed side up to 0.16 at the tail side. The crystal was sliced into several wafers with the thickness of 500 µm perpendicular to the growth direction. In the following discussion, the wafers are referred to as S2 through S19, obtained from the seed end to the tail end of the ingot crystal, successively, from 2, 3, 6, 16, and 19 cm distances. For better observations of the MRS and OT experiments, both surfaces of the wafers were mirror-polished. The OT measurements were performed from the centers of various wafers at room temperature using the Buker IFS 66v FTIR spectrometer.[19]

The present Raman measurements were carried out at room temperature using a Ranishaw 2000 model micro-Raman spectrometer equipped with an Ar-ion laser operating at 514.5 nm wavelength and a cooled CCD detector. The incident light was focused through a 50× objective lens onto the wafer and the scattered signal was collected with the same lens in the back-scattering geometry. The laser power was sufficiently low to prevent the local heating of the sample. To suppress the Rayleigh scattering light and the background noise, a suitable notch filter was used and the slit width was reduced to about 100 µm. In order to increase the accuracy of MRS measurement, all the spectra were recorded together with fluorescence lines from a Ne lamp for calibration.

3.2 MRS experimental results

3.2.1 Si–Si peak position at the center of the wafer

First-order Raman spectra from $Si_{1-x}Ge_x$ typically show Si–Si, Si–Ge, and Ge–Ge phonon modes. Besides these phonon modes, some weak peaks are also observed in the spectra. The apperance of the phonon modes depends on the compositional fraction.[20,21] Raman spectra measured at the centers of the front and back surfaces of various wafers showed a prominent Si–Si phonon peak and several weak peaks. The spectra have been shown in our another study.[22] Since the investigated wafers were Si-rich, the Ge–Ge phonon peak did not appear in the spectra. Here, we have discussed the Si–Si peak position because it was sharp and strong in the spectra. It is found in Fig. 3 that the Si–Si peak positions vary gradually from wafer to wafer along the crystal growth direction, although they are found to be almost the same both from the front and back surfaces of an individual wafer. This indicates that there is a gradual variation of composition along the crystal length, but almost uniform composition along the thickness of an individual

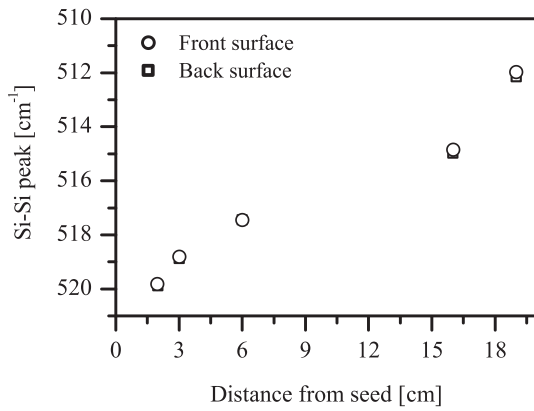

Fig. 3. Si–Si peak positions measured from the center of the front and back surfaces of various wafers.

wafer. Since the compositional variation is gradual along the length of the crystal and the wafers were sliced about 500 μm thick, the compositional variation along the growth direction for an individual wafer is very small and can be neglected.

3.2.2 *Si–Si peak position along the diameter and near the corner of the wafer*

In order to understand the radial compositional profile, Raman spectra were measured along the arrows denoted by D1 and D2 in Fig. 4. Figure 5 shows the variation of Si–Si peak positions along the diameter of various wafers. It is found in Fig. 5 that the Si–Si peak positions are almost the same along the D1 and D2 directions of the wafers S2, S3, and S6. In contrast, they vary symmetrically along the D1 and D2 directions of the wafers S16 and S19. Furthermore, the Si–Si peak positions are found to be identical in both the directions and shifted by about 2.6 and 3.5 cm^{-1} as one moves away from the center to the edge of the wafers S16 and S19, respectively. Therefore, the MRS experimental results demonstrate that there exists homogeneous composition in the wafers S2 to S6. On the other hand, the wafer S16 has a symmetrical compositional profile with flat near the center. However, a radial symmetry in the parabolic compositional profile exists in the wafer S19.

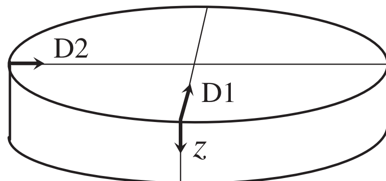

Fig. 4. Schematic of the wafer and the arrows along which MRS measurements were made.

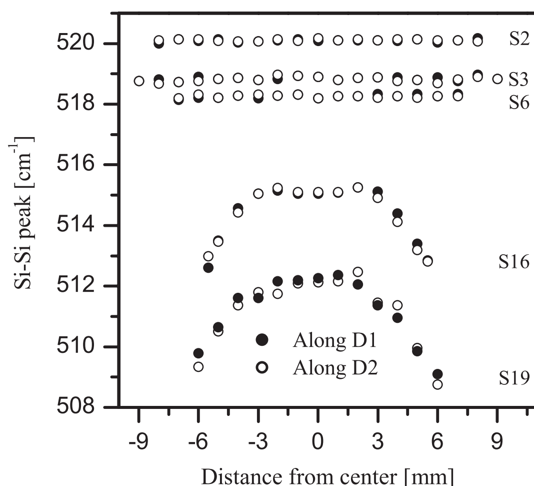

Fig. 5. Si–Si peak positions along the diameter of various wafers.

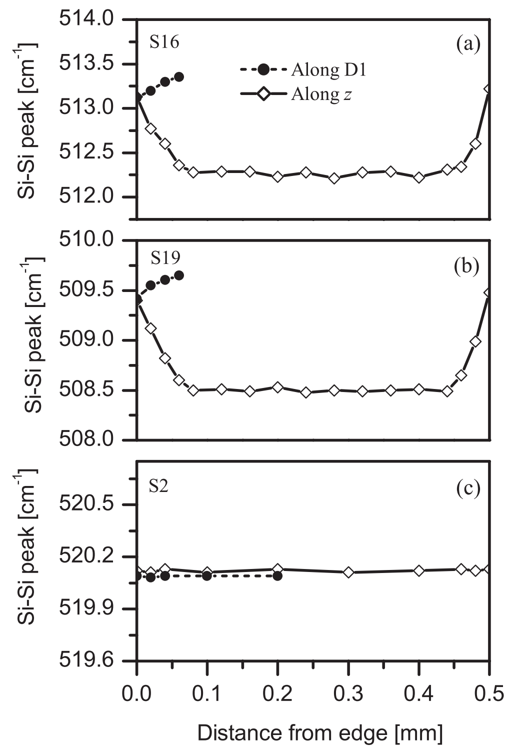

Fig. 6. Si–Si peak positions measured at an interval of 20 μm along the D1 and z directions of (a) wafer S16, (b) wafer S19, and (c) wafer S2. The measurement schematic is shown by arrows in Fig. 4.

In order to confirm the existence of strain in the wafers, precise Raman measurements were further performed at an interval of 20 μm along the D1 and z directions, as indicated in Fig. 4. Figures 6(a) and 6(b) show the Si–Si peak positions measured from the wafers S16 and S19, respectively. It is found in Fig. 6(a) that the measurements at the corners along both directions give the same results; however, when measured away from the corner, a shift is observed between the phonons measured from the two directions. In the D1 direction, the phonon shifts towards higher energy. Only few experimental points are shown to understand the behavior of the phonon shift. The complete profile is the same as that in Fig. 5. On the other hand, the phonons measured along the z direction shift rapidly in the lower energy direction by 0.80 cm^{-1} for about 70 μm, after which the phonon position becomes almost constant until the vicinity of 70 μm from the other corner along the z direction. At both corners along the z direction, the phonon positions are almost the same. Similar results with a maximum shift of 1.0 cm^{-1} are also found for the wafer S19 in Fig. 6(b). Since the compositional variation along the z direction is almost negligible, the phonon shift found along the z direction of the wafer is solely connected to the strain effect. Further-

more, the same phonon shift at the corners along the z direction may have resulted from the relaxation of strain due to the edge effect. To confirm these experimental results, similar measurements were performed in the wafer S2, which has a flat compositional profile and hence is free from strain. The results are presented in Fig. 6(c). Interestingly, there is no shift in the Si–Si vibration for measurements performed along the D1 and z directions, which indicates that the shifts in Figs. 6(a) and 6(b) are solely connected to the strain.

3.3 Strain effect on MRS

Under the influence of strain, the optical phonon splits into three phonon modes at $q \approx 0$ in cubic crystals such as Si and GaAs. The frequencies of these phonon modes are shifted by the amounts of $\Delta\Omega_i$ ($i = 1$ to 3) from the unstrained phonon frequency Ω_0. Since the wafers are assumed to be thin, the strain components related to the z can be neglected. Therefore, in-plane strain analysis can be applied in the wafers under investigation. According to the dynamic secular equation derived by Anastassakis,[23] the strain-induced shifts in the present strain case can be represented by

$$\Delta\Omega_1(r) = \frac{1}{4}\left\{(\tilde{K}'_{11} + \tilde{K}'_{12})[\varepsilon_{rr}(r) + \varepsilon_{\theta\theta}(r)] + (\tilde{K}'_{11} - \tilde{K}'_{12})[\varepsilon_{rr}(r) - \varepsilon_{\theta\theta}(r)]\cos 2\theta\right\}\Omega_0, \quad (10)$$

$$\Delta\Omega_2(r) = \frac{1}{4}\left\{(\tilde{K}'_{11} + \tilde{K}'_{12})[\varepsilon_{rr}(r) + \varepsilon_{\theta\theta}(r)] - (\tilde{K}'_{11} - \tilde{K}'_{12})[\varepsilon_{rr}(r) - \varepsilon_{\theta\theta}(r)]\cos 2\theta\right\}\Omega_0, \quad (11)$$

where $\tilde{K}'_{11}$ and $\tilde{K}'_{12}$ are the phonon deformation potentials (PDPs) in the ⟨111⟩ direction of the crystal. θ is the angle between the crystallographic axis and the direction of the crystal face on which the experiments were performed. On account of axial symmetry if the θ dependence is neglected, the above equations become

$$\Delta\Omega_1(r), \Delta\Omega_2(r) = \frac{1}{4}\left\{(\tilde{K}'_{11} + \tilde{K}'_{12})[\varepsilon_{rr}(r) + \varepsilon_{\theta\theta}(r)]\right\}\Omega_0. \quad (12)$$

Thus, phonon frequency under strained condition can be expressed by

$$\Omega(r) = \Omega_0(x) + \Delta\Omega_i(r), \quad (13)$$

where $\Omega_0(x)$ is the compositional dependence of phonon frequency under unstrained condition. For Si–Si phonon, it is given[20] by

$$\Omega_0(x) = 521 - 70x. \quad (14)$$

The experimental values of PDP are available[23] in the ⟨100⟩ direction. In our experiments, since the laser beam was probed parallel to the ⟨111⟩ along the D1 and D2 directions, the PDPs of $\tilde{K}'_{11}$, $\tilde{K}'_{12}$, and $\tilde{K}'_{44}$ are evaluated in the ⟨111⟩ direction using tensor rotation technique.[23] In order to determine the strain contribution on MRS results, the PDPs for $Si_{1-x}Ge_x$ crystal are determined by linear interpolation between the values of Si and Ge crystals listed in Table II. By substituting eqs. (7) and (8) into eq. (12), the compositional dependence of strain-induced shift can be determined along the diameter of the wafer. For the parabolic and flat-center parabolic compositional profiles, the strain-induced shifts can be represented by

Table II. PDPs of $\tilde{K}_{11}$, $\tilde{K}_{12}$, and $\tilde{K}_{44}$ are available in the ⟨100⟩ direction for Si and Ge crystals.[23] PDPs of $\tilde{K}'_{11}$, $\tilde{K}'_{12}$, and $\tilde{K}'_{44}$ are calculated in the ⟨111⟩ direction using the tensor rotation technique.[23]

	⟨100⟩			⟨111⟩		
Crystal	$\tilde{K}_{11}$	$\tilde{K}_{12}$	$\tilde{K}_{44}$	$\tilde{K}'_{11}$	$\tilde{K}'_{12}$	$\tilde{K}'_{44}$
Si	−1.85	−2.30	−0.70	−2.77	−1.99	0.0
Ge	−1.45	−1.95	−1.10	−2.80	−1.50	0.0

$$\Delta\Omega(\text{center}) = -8.44x_c,$$

and

$$= -3.84x_c, \quad (15)$$

respectively, at the wafer center. Similar results at the wafer edge can be represented by

$$\Delta\Omega(\text{edge}) = -15.24x_e,$$

and

$$= -10.25x_e, \quad (16)$$

where x_e is the composition at the edge of the wafer. For deriving eqs. (15) and (16), the parameters in eq. (9) are adjusted to fit the experimental data shown in Fig. 5 for the wafers S16 and S19. With the combination of eqs. (13)–(16), the compositional dependence of Si–Si phonon frequency at the wafer center can be given by

$$\Omega(\text{center}) = 521 - 78.44x_c,$$

and

$$= 521 - 73.84x_c, \quad (17)$$

respectively, for the parabolic and flat-center parabolic compositional profiles. Similar results at the wafer edge can be given by

$$\Omega(\text{edge}) = 521 - 85.24x_e,$$

and

$$= 521 - 80.25x_e. \quad (18)$$

In the same manner, the compositional dependence of Si–Si phonon frequency can be derived for each measurement point along the radial direction of the wafer, which can be used to evaluate the composition from the phonon positions measured along the radial direction of the wafers S16 and S19.

3.4 Strain effect on OT

The influence of strain on OT results can be determined by analyzing the electronic energy bands under strained condition. The strain-induced splitting of the heavy-hole and light-hole valence bands was investigated previously.[16,17] Following the solution of the orbital strain Hamiltonian[17] for $k = 0$, the strain-induced change in energy gap, ΔE, involving the $j = 3/2$ valence bands can be represented in the present strain case:

$$\Delta E(r) = \frac{1}{2}[\varepsilon_{rr}(r) + \varepsilon_{\theta\theta}(r)](2a_v \pm b_v), \quad (19)$$

where a_v is the hydrostatic potential and b_v is the shear deformation potential. b_v is associated with strain of

Table III. Hydrostatic and shear deformation potentials for Si and Ge crystals.[24,25)]

	Si	Ge
Hydrostatic deformation potential, a_v (eV)	−2.46	−8.1
Shear deformation potential, b_v (eV)	−2.35	−2.9

tetragonal symmetries, which removes the degeneracy of the bands as indicated by the ± sign.

In order to determine the influence of strain on OT results, the electron deformation potentials for $Si_{1-x}Ge_x$ mixed material are calculated by linear interpolation between the values listed for Si and Ge crystals in Table III. By using eq. (19), the compositional dependence of band gap energy under strained condition can be represented by

$$E_g^s(r) = E_g(x) + \Delta E(r), \tag{20}$$

where $E_g(x)$ is the compositional dependence of excitonic band gap energy under unstrained condition. For the $Si_{1-x}Ge_x$ crystal, the $E_g(x)$ can be given[19)] by

$$E_g(x) = 1.11 - 0.382x \tag{21}$$

at room temperature. In a previous study,[26)] the compositional dependence of excitonic band gap energy was given by $1.15 - 0.43x + 0.206x^2$ in unstrained $Si_{1-x}Ge_x$ for the composition range $0 \leq x \leq 0.85$ from low-temperature photoluminescence measurements. In this study, the excitonic band gap energy was varied linearly with composition for the composition range $0 \leq x \leq 0.2$. Since OT measurements were carried out at room temperature and the composition range in the investigated samples was $0 \leq x < 0.2$, we have used eq. (21) to explain OT experimental results. By substituting eqs. (7) and (8) into eq. (19), the compositional dependence of ΔE can be represented by

$$\Delta E(\text{center}) = -0.09x_c,$$

and

$$= -0.028x_c \tag{22}$$

at the wafer center for parabolic and flat-center parabolic compositional profiles, respectively. By combining eqs. (20)–(22), the compositional dependence of excitonic band gap energy under strained condition can be given by

$$E_g^s(\text{center}) = 1.11 - 0.472x_c,$$

and

$$= 1.11 - 0.41x_c \tag{23}$$

at the wafer center for the parabolic and flat-center parabolic compositional profiles, respectively. By using eq. (23), the composition at the wafer center can be determined from the OT data measured from the wafers S16 and S19.

3.5 Comparison between MRS and OT results

By using unstrained eqs. (14) and (21), the compositions from the center of various wafers are determined both from the MRS and OT data, respectively. The results are listed in Table IV. It is found in Table IV that the compositions evaluated from the center of the wafers S2 to S6 are in excellent agreement. However, they show poor agreement in the wafers S16 and S19. Since there is no strain in the wafers S2 to S6 due to homogeneous composition, the unstrained equations give us good results. In contrast, the existence of strain was confirmed in the wafers S16 and S19 due to the flat-center parabolic and parabolic compositional profiles, respectively. Therefore, the discrepancy between the MRS and OT compositions evaluated by the unstrained equations is a result of the strain induced by the compositional variation in the wafers S16 and S19.

Table IV. Si–Si peak position and excitonic band gap energy were measured from the centers of various $Si_{1-x}Ge_x$ wafers by MRS and OT experiments. MRS and OT compositions were evaluated using eqs. (14) and (21), respectively, which were determined from unstrained $Si_{1-x}Ge_x$.[19,20)]

Sample no.	Si–Si (cm^{-1})	$E_g(x)$ (eV)	MRS composition	OT composition
S2	520.02	1.104	0.014	0.014
S3	518.93	1.098	0.030	0.030
S6	517.29	1.089	0.053	0.054
S16	515.20	1.077	0.082	0.085
S19	512.18	1.057	0.126	0.137

Furthermore, by considering the strain effect on the MRS data, the compositions are evaluated using eq. (17) for the wafers S16 and S19. The results were determined to be 0.079 and 0.112 from the center of the wafers S16 and S19, respectively, which deviate by about 7.6 and 22% from those obtained from the OT measurements. In a previous study,[19)] the OT compositions were evaluated from the excitonic band gap energy without considering the strain effect at that time. In the present study, the existence of tensile strain is confirmed in the wafers S16 and S19 from the strain model as well as from the MRS measurements. Under the tensile strain condition, the OT measurement may give us a higher composition if it is estimated using eq. (21). Including the strain effect on the OT results, we have further evaluated the compositions from the center of the wafers S16 and S19 using eq. (23) and the results are found to be 0.080 and 0.112, which are almost the same as those evaluated from the MRS data. A comparison between the MRS and OT compositions is shown in Fig. 7 for the wafers S2 to S19. The results are found to be in good agreement.

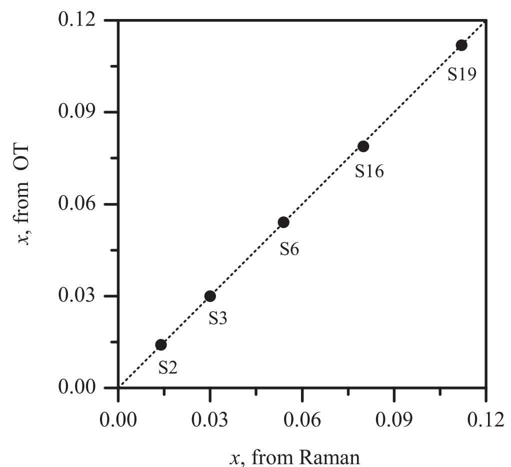

Fig. 7. Comparison between the compositions evaluated at the center of the wafers from both the RS and OT data.

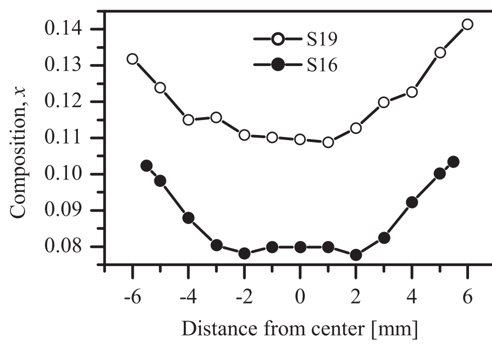

Fig. 8. Compositional profiles along the radial direction of the wafers S16 and S19.

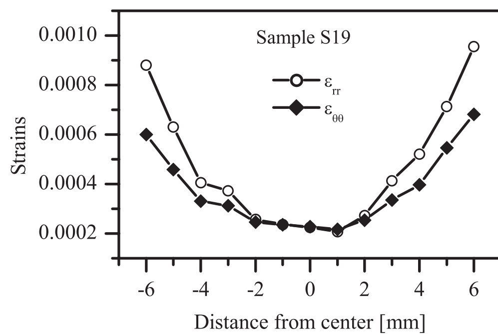

Fig. 9. Radial and tangential strain distributions along the radial direction of the wafer S19.

3.6 Residual strain and alloy composition

Using the strain model, we have already presented eqs. (17) and (18), which were obtained at the wafer center and edge under strained condition for the parabolic and flat-center parabolic compositional profiles. Similar equations were derived for each measurement point and applied to evaluate the compositional profiles along the radial direction of the wafers S16 and S19. The results are shown in Fig. 8. It is found in Fig. 8 that the estimated compositional profiles vary from 0.078 to 0.105 and from 0.112 to 0.143 along the radial direction of the wafers S16 and S19, respectively. By substituting these compositional profiles into eqs. (7) and (8), both radial and tangential strain distributions can be determined. Figure 9 shows the radial and tangential strain distributions evaluated for the wafer S19. The radial and tangential strains are found to vary from 2.27×10^{-4} to 9.58×10^{-4} and from 2.27×10^{-4} to 6.82×10^{-4}, respectively, for the parabolic variation of composition from 0.112 to 0.143 along the radial direction of the wafer S19. Similar results were varied from 1.22×10^{-4} to 6.31×10^{-4} and from 1.22×10^{-4} to 4.38×10^{-4}, respectively, for the flat-center parabolic variation of composition from 0.078 to 0.105 along the radial direction of the wafer S16. By substituting these strain values into eq. (12), the strain-induced shifts are determined to be approximately 0.75 and $1.01\,\mathrm{cm}^{-1}$ near the edge of the wafers S16 and S19, respectively. These strain-induced shifts show good agreement with those of 0.80 and $1.0\,\mathrm{cm}^{-1}$, which were measured by MRS experiments near the corners of the wafers S16 and S19, respectively, due to the strain relaxation effect. In this study, the strain model is applied to evaluate the strain components in bulk $Si_{1-x}Ge_x$ mixed crystal. However, it can be used to investigate strain components in bulk mixed crystals having the symmetrical variation of composition along the radial direction and uniform composition along the growth direction.

4. Conclusions

A radially symmetrical strain model has been developed in wafer-shaped bulk mixed crystals by assuming a symmetrical variation of composition along the radial direction and uniform composition along the growth direction. The model was applied to investigate the residual strain distribution in bulk $Si_{1-x}Ge_x$ mixed crystal for the parabolic and flat-center parabolic compositional profiles. The amount of strain and its distribution were found to be strongly dependent on the compositional profile and its range. The radial and tangential strains were varied from 3.59×10^{-4} to 1.08×10^{-3} and from 3.59×10^{-4} to 6.3×10^{-4}, respectively, for the parabolic variation of composition from 0.0 to 0.05 from the center to the edge of the wafer. On the other hand, for the same range of the flat-center parabolic profile, they were varied from 1.84×10^{-4} to 9.94×10^{-4} , and from 1.84×10^{-4} to 3.93×10^{-4}. The results obtained from the model were confirmed by the MRS and OT experiments performed in various $Si_{1-x}Ge_x$ wafers. The experimental results demonstrated that the existence of strain was related to the radial compositional variation in the wafers. With the combination of the strain model and MRS experiments, the compositions evaluated from the MRS data were found to deviate by approximately 7.6 and 22% from those evaluated from the OT data under unstrained condition. Furthermore, by considering the strain effect on OT measurements, the compositions evaluated from the OT data were in excellent agreement with those estimated from the MRS data. Furthermore, in conjunction with the strain model and MRS experimental results, both strain distributions and compositional profiles were determined. In addition, the strain-induced shifts evaluated from the strain values were found to be in good agreement with those obtained near the corner of the wafers due to the strain relaxation effect. In this study, the model was used to determine the strain components in the bulk $Si_{1-x}Ge_x$ crystal as an example. However, it can be used to determine strain components in bulk mixed crystals for various compositional profiles having a symmetrical variation along the radial direction and uniform composition along the growth direction.

Acknowledgment

The authors gratefully acknowledge to Professor Dr. W. Schröder for supplying the $Si_{1-x}Ge_x$ wafers used in this study.

1) A. Erko, F. Schäfers, W. Gudat, N. Abrosimov, V. Alex, S. Rossolenko and W. Schröder: Nuclear Instrum. Methods Phys. Res. A **374** (1996) 408.
2) S. Keitel, C. Retsch, T. Niemöller, J. Schneider, N. Abrosimov, S. Rossolenko and H. Riemann: Nuclear Instrum. Methods Phys. Res. A **414** (1998) 427.
3) A. Erko, N. V. Abrosimov and V. Alex: Cryst. Res. Technol. **37** (2002) 685.
4) S. Zollner, R. Liu, Q. Xie, M. Canonico, S. Lu, M. Kottke, X. D. Wang, A. Volinsky, M. Sadaka, T. White, A. Barr, S. Thomas and

B. Y. Nguyen: Invited paper at the Int. Symp. on Compound Semiconductors, San Diego, CA, USA, IEEE Catalog No. 03TH8675, 2003, p. 183.

5) M. R. Islam, M. Yamada, N. V. Abrosimov, M. Kiyama and M. Tatsumi: to be published in Eur. Phys. J. AP.

6) M. R. Islam, A. Hiroki and M. Yamada: Jpn. J. Appl. Phys. **43** (2004) 1088.

7) A. Bensaada, A. Chennouf, R. W. Cochrane, J. T. Graham, R. Leonelli and R. A. Masut: J. Appl. Phys. **75** (1994) 3024.

8) T. D. Harris, M. G. Lamont, R. Sauer, R. M. Lum and J. K. Klingert: J. Appl. Phys. **64** (1988) 5110.

9) H. Asai and K. Oe: J. Appl. Phys. **54** (1983) 2052.

10) J. M. Gilpérez, F. Gonzalez-Sanz, E. Calleja, E. Muñoz, J. M. Calleja, N. Mestres, J. CastagnÕ and E. Barbier: Semicond. Sci. Technol. **7** (1992) 562.

11) S. P. Timoshenko and J. N. Goodier: *Theory of Elasticity* (McGraw-Hill, New York, 1970) 3rd ed., Chap. 14, p. 406.

12) H. F. Wolf: *Semiconductors* (Pergamon Press, Oxford, 1969) Chap. 1, p. 128.

13) M. R. Islam, P. Verma, M. Yamada, S. Kodama, Y. Hanaue and K. Kinoshita: Mater. Sci. Eng. B **91–92** (2002) 66.

14) M. R. Islam, P. Verma and M. Yamada: *Advanced Nanomaterials and Nanodevices*, ed. H. Gao, H. Fuchs and D. Chen (IOP Publishing, 2003) p. 912.

15) N. Usami, T. Takahashi, K. Fujiwara, T. Ujihara, G. Sazaki, Y. Murakami and K. Nakajima: Jpn. J. Appl. Phys. **41** (2002) 4462.

16) D. H. Rich, A. Ksendzov, R. W. Terhune, F. J. Grunthaner, B. A. Wilson, H. Shen, M. Dutta, S. M. Vernon and T. M. Dixon: Phys. Rev. B **43** (1991) 6836.

17) F. H. Pollak and M. Cardona: Phys. Rev. **172** (1968) 816.

18) J. Wollweber, D. Schulz and W. Schröder: J. Cryst. Growth **163** (1996) 243.

19) A. Gerhardt: Proc. Mater. Res. Soc. Symp. **450** (1997) 451.

20) M. I. Alonso and K. Winer: Phys. Rev. B **39** (1989) 10056.

21) M. Frank, K. F. Dombrowski, H. Rücker, B. Dietrich and K. Pressel: Phys. Rev. B **59** (1999) 10614.

22) M. R. Islam and M. Yamada: to be published in IOP Conf. Ser. Book.

23) D. J. Lockwood and J. F. Young: *Light Scattering in Semiconductor Structures and Superlattices* (Plenum Press, New York, 1991) p. 173.

24) I. Balslev: Solid State Commun. **5** (1967) 315.

25) C. G. Van de Walle: Phys. Rev. B **39** (1989) 1871.

26) J. Weber and M. I. Alonso: Phys. Rev. B **40** (1989) 5683.